sustainability

MDPI

Article

Analysis and Experimental Study on the Influence of Louver Separation Device on the Sand Collection Efficiency of Wind Erosion Instrument

Zhentong Liu [1], Fengwu Zhu [1], Dongyan Huang [1], Man Ao [2], Yunhai Ma [3] and Xianzhang Meng [1,*]

[1] College of Engineering and Technology, Jilin Agricultural University, Changchun 130118, China; liuzhentong@mails.jlau.edu.cn (Z.L.); zhufengwu@jlau.edu.cn (F.Z.); huangdy@jlu.edu.cn (D.H.)
[2] Northeast Institute of Geography and Agroecology, Chinese Academy of Sciences, Changchun 130102, China; aoman@iga.ac.cn
[3] College of Biological and Agricultural Engineering, Jilin University, Changchun 130021, China; myh@jlu.edu.cn
* Correspondence: teachermxz@jlau.edu.cn; Tel.: +86-13504468265

Abstract: A wind erosion instrument is a core instrument for collecting sand particles in wind and sand flows and studying the laws of wind and sand movement. To study the influence of the internal structure of the wind erosion instrument on its sand collection efficiency, a built-in louver separation device was designed. Based on CFD and Fluent 2022 software, numerical analysis was conducted using an RNG k-ε model, and the discrete phase model (DPM) method was used to calculate the sand collection efficiency. The flow field analysis of the new wind–sand separator was carried out. The influence of blade inclination angle, blade thickness, and blade number on sand collection efficiency was studied using single-factor and response surface analysis methods. The optimal parameter combination was obtained as blade inclination angle of 30°, blade thickness of 1.25 mm, and blade number of 10. A simulation model was established based on the optimal combination parameters, and the performance of the wind erosion instrument before and after the addition of the louver separation device was compared. The simulation results show that adding a louver separation device can increase static pressure, alleviate short-circuit flow and back-mixing phenomena, and stabilize the flow field; increasing tangential velocity leads to an increase in particle centrifugal force; reduce axial velocity, prolong particle stagnation time, and minimize particle escape. The particle trajectory pattern is mostly a continuous spiral path, which is conducive to capturing particles and improving sand collection efficiency. Compared with the original structure, for particles with diameters ranging from 0.001–0.05 mm, 0.005–0.01 mm, 0.01–0.05 mm, 0.05–0.1 mm, and 0.1–0.5 mm, the addition of a louver separation device increased the sand collection efficiency by 32.74%, 22.55%, 33.17%, 11.45%, and 0.13%, respectively. When the wind speed is 13.8 m/s and the diameter range is 0.001–0.5 mm, the average sand collection efficiency obtained from simulation tests and wind tunnel tests is 86.18% and 84.32%, respectively, with an error of 2.2%. The simulation results are reliable. The research results show that adding a louver separation device can improve the sand collection efficiency of the wind erosion instrument, and has better overall performance compared to the original wind–sand separator. This study provides a basis for further research on the structure of wind erosion gauges and the environmental protection of farmland. Strengthening land management can effectively protect soil resources, reduce wind erosion, ensure the stability of the ecosystem, and lay the foundation for promoting the sustainable use of land.

Keywords: soil wind erosion; wind erosion instrument; louvre separation device; sand collection efficiency

Citation: Liu, Z.; Zhu, F.; Huang, D.; Ao, M.; Ma, Y.; Meng, X. Analysis and Experimental Study on the Influence of Louver Separation Device on the Sand Collection Efficiency of Wind Erosion Instrument. *Sustainability* **2024**, *16*, 10071. https://doi.org/10.3390/su162210071

Academic Editor: Teodor Rusu

Received: 11 October 2024
Revised: 8 November 2024
Accepted: 13 November 2024
Published: 19 November 2024

1. Introduction

Wind erosion of farmland soil is an important cause of soil erosion [1]. Soil wind erosion is the erosion phenomenon caused by external forces dominated by wind, which

blows, jumps, and rolls materials such as dust and sand on the surface of the earth. Severe wind erosion can lead to surface soil erosion, coarsening of texture, and decreased fertility, thereby affecting food security [2,3]. In addition, wind erosion is also the source of sandstorms, and land desertification caused by wind erosion is also an important cause of sandstorms [4]. These ongoing processes have fuelled the annual spread of land degradation globally [5], posing a serious threat to the stability of ecosystems and the sustainable development of human societies. The impacts are not limited to areas such as reduced crop yields and diminished supply of ecosystem services [6], but have far-reaching implications for global sustainable development. Therefore, a reliable assessment of soil wind erosion and an understanding of the dynamics of near-surface wind and sand flow are crucial. These studies provide indispensable tools and insights for the development of soil conservation strategies, thus contributing to the achievement of sustainable land use.

Soil wind erosion is a common problem worldwide [7,8], especially in the arid regions of northern China. It is the most prominent issue facing sustainable agricultural development, and strengthening farmland protection is urgent. In order to effectively control soil wind erosion, it is necessary to clarify its formation mechanism. To this end, it is necessary to develop a device that can collect sand and dust particles carried by the wind during soil erosion [9], namely a wind erosion instrument. Wind erosion instrument, also known as sand collection instrument, is a commonly used equipment for field wind erosion observation and wind tunnel experiments [10,11]. Its different structural characteristics directly affect the determination of sand transport rate and the study of wind and sand flow field structure [12]. Therefore, it is necessary to study the structure of wind erosion instruments. Wind erosion data recording and assessment can scientifically formulate treatment and restoration measures and prevent environmental damage, thereby maintaining ecological balance, ensuring the health and stability of the ecosystem, effectively curbing the further spread of wind erosion, protecting land resources and achieving sustainable development.

The earliest wind erosion sand collector was designed by Bagnold [13]. Subsequently, Fryear [14] and Kuntze [15] designed BSNE and SUSTRA wind erosion sand collectors with exhaust and rotating guidance devices, which can meet the needs of field wind erosion observation. Wilson S J and Cooke R U [16] improved the sand and dust collector, enabling it to collect sand samples of different heights at the same location, with good wind direction directionality and high sand collection efficiency. Song Tao et al. [17] designed a Shunthedging and Multi-stage Expansion Combined Sand Sampler, which can achieve wireless transmission and automatic data collection. Prandtl et al. [18] installed blades on the vortex detector of a cyclone separator, and the introduction of blades significantly reduced the turbulence level of the internal airflow, converting its kinetic energy into pressure energy and effectively reducing pressure loss. These studies not only provide valuable guidance for the management of soil wind erosion, but also lay the foundation for the development of sustainable land conservation strategies.

The Fluent platform provides flexible mesh features, allowing for structured and unstructured mesh partitioning of geometric shapes [19]. Hou Jianlong [20] studied the cyclone separator in high-pressure systems using the RNG k-ε model on the Fluent platform. Liu Shuyan et al. [21] applied the Reynolds stress model to analyze the tangential and axial velocities on different sections of a cyclone separator. Li et al. [22] proposed a cyclone separator composed of spiral guide vanes, which can effectively improve the distribution of the flow field, and the pressure drop and tangential velocity increase with the increase of the number of spiral guide vane turns, thus improving the sand collection efficiency.

The wind–sand separator is the core component of the wind erosion instrument, and its performance determines the testing accuracy of the wind erosion instrument. In order to improve the performance of the wind erosion instrument, a louver separation device was added inside the wind erosion separator in this paper. Based on the Fluent platform, a combination of CFD numerical simulation and wind tunnel test verification was used to compare the influence of louver separation devices with different structural parameters on the performance of the wind erosion instrument, understand the internal airflow movement

law of the wind erosion instrument, and further improve the sand collection efficiency. In addition, an automatic weighing device has been installed at the bottom of the wind–sand separator to improve the testing accuracy of wind erosion data and optimize the structure of the wind erosion instrument. This device can also achieve automatic collection of wind erosion data from multiple measurement points, providing a foundation for further research on wind erosion instruments.

2. Materials and Methods

2.1. Numerical Model Explanation

2.1.1. Overall Structure and Working Principle of Wind Erosion Instrument

The overall structure of the wind erosion instrument is composed of a guide plate, rotating shaft, five sand collecting units, a fixing rod of the sand collecting unit, a fixing rod of the wind erosion instrument, a fixing rod flange of the wind erosion instrument, and other components. As shown in Figure 1, the guide plate is installed on the top of the fixing rod of the wind erosion instrument, and the embedded parts are installed at the bottom, connected with the fixed rod flange, and buried deeply underground to ensure the stability of the wind erosion instrument in strong wind weather.

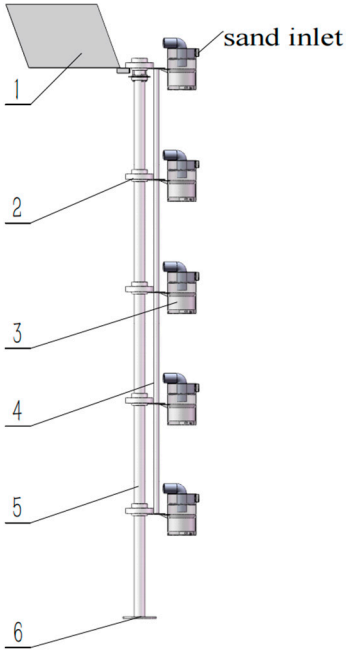

Figure 1. Overall structure of wind erosion instrument: 1. guide plate; 2. rotating shaft; 3. sand collection unit; 4. fixing rod of sand collecting unit; 5. fixing rod of wind erosion instrument; 6. fixing rod flange of wind erosion instrument.

When the wind erosion instrument is in the sandstorm flow environment, the guide plate will be driven by the wind. Under the joint action of the guide plate, the rotating shaft, and the fixing rod of the sand collecting unit, the sand collection unit at each height will rotate in the same direction synchronously, so that each sand inlet of the wind erosion instrument is always aligned in the incoming wind direction. In this way, sand samples of different heights can be collected at a single point to reduce the problem of uneven arrangement and improve the efficiency of sand collection.

2.1.2. Structure and Working Principle of the Sand Collection Unit

The sand collection unit is an important structure of the wind erosion instrument dust collector, which includes the upper wind–sand separator, the lower collection box, and the automatic weight measuring system. The design of the wind–sand separator of different structures can reduce the sand carrying capacity of the sand flow in the instrument, realize

the sand separation, and improve the sand gathering efficiency. Compared with other types of sand-gathering instruments, the wind–sand separator in the sand collection unit breaks through the previous idea of reducing speed through single capacity expansion, puts forward the idea of a cylindrical winding flow structure, and designs the louver separation device to improve the efficiency of sand gathering. A diagram of its structure composition is shown in Figure 2.

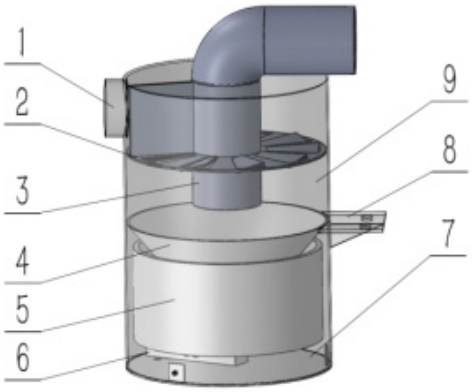

Figure 2. Structural diagram of sand collection unit: 1. inlet pipe; 2. louver separation device; 3. exhaust pipe; 4. cone-shaped guide plate; 5. collection box; 6. weight sensor; 7. bottom cover; 8. shell fixing bracket; 9. shell.

During the operation, the dust in the sand flow enters the sand separator of the sand collecting unit through the gas inlet of the intake pipe. Under the action of the louver separation device, the cylindrical flow is moved to change the airflow speed and realize the separation of the sand. The gas flows out from the exhaust port, and the dust falls into the collection box. The weighing sensor collects the quality of the dust and is processed through an automated data collection system. Finally, the real-time weight of the dust in the collection box will be displayed on the data page, so as to realize the remote measurement of soil erosion, meet the needs of field observation, save manpower, and improve efficiency.

2.1.3. Design Principle of Louver Separation Device

The louver separation device is designed based on the principle of cylindrical flow, by setting a diversion baffle structure at the end of the inlet pipe, forcing the airflow to rotate around the outer wall of the exhaust pipe after passing through the baffle, in order to achieve a change in airflow velocity. As shown in Figure 3a, when the airflow passes through the separator, it starts to move clockwise after being acted upon by the baffle at point A, forming a boundary layer flow between the outer wall of the exhaust pipe and the inner wall of the wind–sand separator. At point B, the airflow velocity reaches its maximum value, and vortices are generated near point C [23], resulting in a significant change in airflow velocity.

The boundary layer is mainly characterized by adhesive flow, and the velocity decreases as it approaches the wall. The airflow separates at the tail of the boundary layer, resulting in vortices; outside the boundary layer, there is mainly free flow, and vortices also appear at the tail of the flow, as shown in Figure 3b. When a vortex occurs, a part of the airflow forms a countercurrent under the reverse gradient and interacts with the subsequent airflow. Assuming the force is F, within the time $\Delta t > 0$, there exists an impulse $F \cdot \Delta t > 0$. According to the law of conservation of momentum $F \cdot \Delta t = m \cdot \Delta v$, it can be inferred that there exists momentum $m \cdot \Delta v > 0$. This indicates that momentum loss occurs during the interaction of airflows, resulting in a decrease in airflow velocity. However, according to the N-S formula, the dissipation due to mixing effects (Reynolds stress) or external forces (physical force) or viscosity is small and negligible.

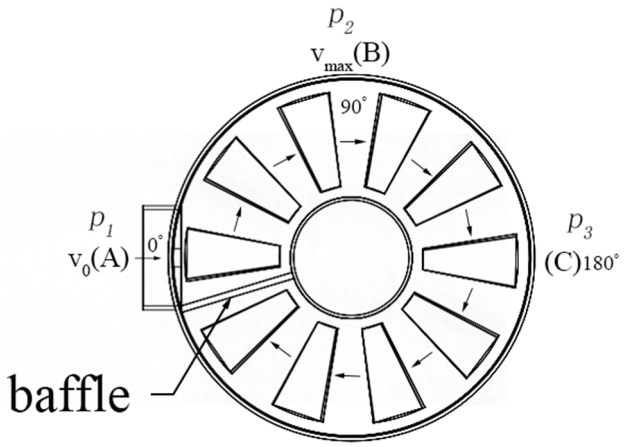

(**a**)

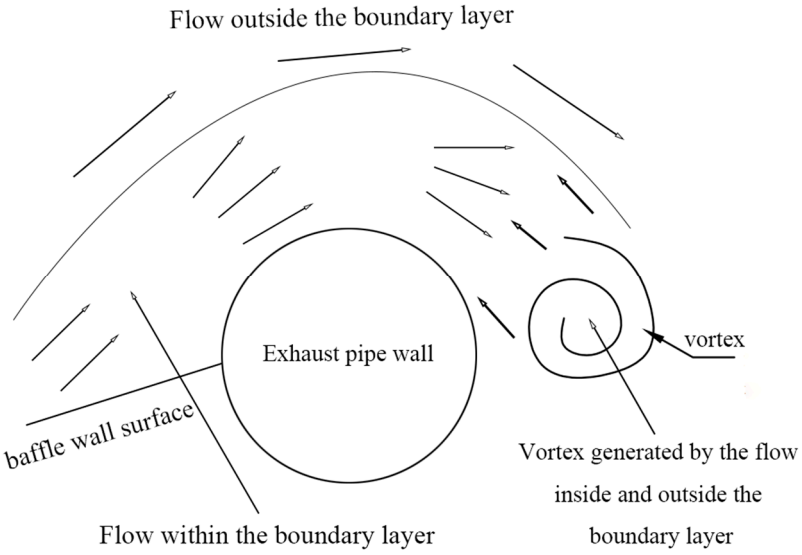

(**b**)

Figure 3. Design schematic of louver separation device: (**a**) Flow-around schematic; (**b**) Flow-around phenomenon.

From the formula of pressure coefficient of cylindrical flow, it is obtained as follows

$$C_p = 1 - 4sin^2\theta \tag{1}$$

It can be seen that the pressure p of the airflow decreases and then increases with the coordinate θ from 0° to 180° in the process of winding. As shown in Figure 2, there exists $p_2 < p_3$, and then the Bernoulli's equation has the following formula:

$$p + \frac{1}{2}\rho v^2 + \rho g h = c \tag{2}$$

where c is a constant, the pressure p is inversely proportional to the velocity v; when the pressure p increases, the velocity of the airflow decreases. This means that the velocity of the airflow decreases when θ goes from 90° to 180° (i.e., around the flow to the back of the cylinder). It can be seen that as long as the structure meets the conditions for cylindrical bypass, the airflow will undergo a velocity reduction behind the structure.

2.2. Numerical Calculation Model and Boundary Condition Setting

2.2.1. Structural Model of Wind–Sand Separator

The fluid calculation basin selected in the numerical simulation calculation is the wind–sand separator in the sand collection unit, which is mainly composed of an inlet pipe, a louver separation device, an exhaust pipe, a conical guide plate, and an outer shell. Compared to the previous wind and sand separator, a louver separation device has been added. Under the action of the louver separation device, the wind and sand flow undergoes cylindrical flow, and the airflow velocity first increases and then decreases; Due to the constraints of the outer surface of the flow structure and the outer shell of the wind–sand separator, the airflow is inevitably forced to descend. When the wind and sand flow enters the conical guide plate, due to its special structure, the airflow will generate shear force on the conical wall surface. At the same time, the airflow will also be affected by the reaction force of the conical wall surface, which forces the airflow to change its flow direction, even reverse flow, and interact with the subsequent airflow in the downward direction to further change the airflow velocity. At this time, most soil particles will fall through the sand discharge port to the collection box under the action of gravity, and the gas will be discharged from the exhaust port to achieve wind and sand separation.

The schematic diagram of the wind–sand separator is shown in Figure 4. Figure 4a shows the original cylindrical wind–sand separator, and Table 1 lists its detailed dimensions. The geometric shape of the louver separation device is shown in Figure 4b, which can efficiently separate wind and sand inside the instrument and improve sand collection efficiency. Figure 4c shows a cylindrical wind–sand separator with added louver separation device.

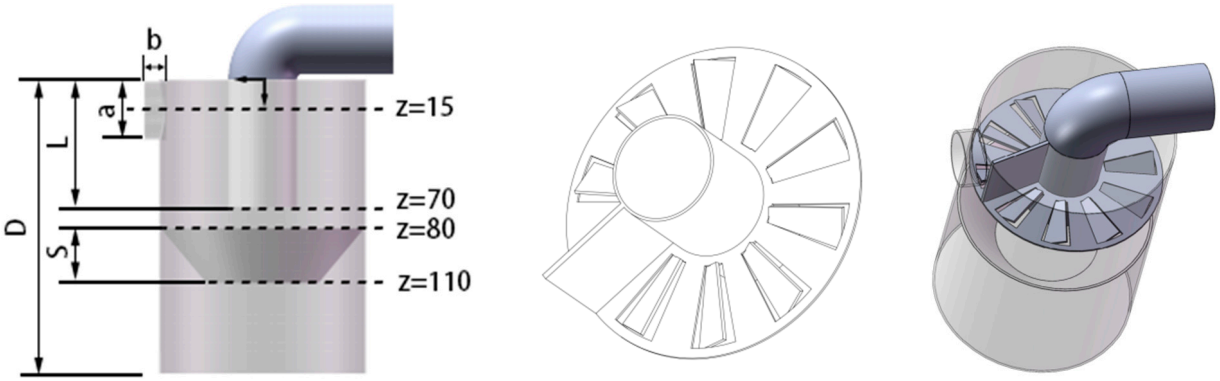

(**a**) (**b**) (**c**)

Figure 4. Wind–sand separator: (**a**) Structural diagram of original wind–sand separator; (**b**) Structural diagram of louver separation device; (**c**) Structural diagram of wind and sand separator with additional louvre separation device.

Table 1. Main dimensions of wind–sand separator.

Parameter.	Size/mm
Inlet pipe diameter a	30
Inlet pipe length b	12
Insertion depth of exhaust pipe L	70
Cone shaped deflector height S	30
Cylinder length D	160

2.2.2. Numerical Method

For simple flow, an increase in the number of equations will lead to an increase in measurement and accuracy, but convergence will deteriorate. However, for complex

turbulent motion, computational characteristics such as high accuracy, low computational complexity, and good convergence are related to the selection of turbulence models [24]. The RNG k-ε turbulence model can simulate complex flow problems such as jet impingement, separation flow, secondary flow, and swirl with high accuracy [25]. Inside the wind–sand separator, due to the influence of airflow and conical wall backflow, a large number of vortices appear in the separator and occupy a certain proportion of the entire flow field. Therefore, the RNG k-ε turbulence model is more suitable.

2.2.3. Boundary Condition Setting

The process of soil wind erosion is generally divided into three stages: particle initiation, particle transport, and particle deposition. The wind speed level directly affects the intensity of soil erosion [26]. Only when the surface wind speed is greater than the starting wind speed of soil erodible particles, can surface soil erodible particles be induced to enter the airflow. According to the wind speed and wind-speed classification standards, weak sandstorms will occur when the wind speed is 5.5–13.8 m/s (4–6 levels). Based on actual working conditions and multiple experiments, it has been found that the inlet velocity of the inlet pipe is too low, and dust does not generate start-up; When the wind speed is too high, sand and dust will escape from the exhaust outlet with the airflow, and the sand collection efficiency of the sand outlet will decrease. Due to the fact that the soil samples taken for subsequent wind tunnel tests are located in Shuangliao City and the common wind speed for wind erosion in spring is above level 6 strong winds (10.8–13.8 m/s) [27], it is reasonable to set the limit value of level 6 strong winds at 13.8 m/s as the inlet wind speed of the inlet pipe for simulation. Under this condition, the structure of the wind–sand separator is optimized to increase the stability of the airflow under strong wind conditions.

Considering that the working condition of the wind–sand separator is a free-flow wind field, the air inlet is set as a velocity inlet. The wind–sand separator has two free outflow outlets (sand discharge outlet and exhaust outlet), and the boundary type should be selected as outflow. The rest of the boundaries are defaulted to walls. ICEM-CFD was used for unstructured mesh partitioning in the fluid computational domain. The partitioned model was imported into the Fluent environment for boundary condition setting, with an inlet velocity of 13.8 m/s, density of 1.225 kg/m^3, and viscosity of 1.8×10^{-5} Pa·s. The RNG k-ε turbulence model was used, with a hydraulic diameter of $d = 4S/L$, where S is the cross-sectional area of the inlet pipe and L is the wetted perimeter. By substituting numerical calculations, the schematic diagram of boundary conditions is shown in Figure 5.

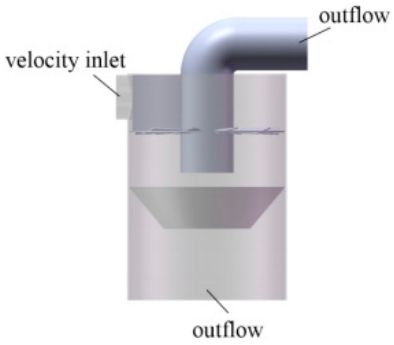

Figure 5. Schematic diagram of boundary conditions for wind–sand separator.

Turbulence intensity:

$$I = 0.16Re^{-\frac{1}{8}} \tag{3}$$

Among them, Re represents the Reynolds number to characterize the flow state of the fluid, and the calculation formula is:

$$Re = \frac{\rho v d}{\mu} \tag{4}$$

In the formula, ρ is the air density, kg/m^3; v is the airflow velocity, m/s; μ is the air viscosity, Pa·s; d is the hydraulic diameter, m.

Substituting each parameter into Equations (3) and (4) yields a turbulence intensity of 4.45% and a hydraulic diameter of 0.03 m.

The sand collection effect was tested based on the capture rate, and the simulation results were compared and analyzed. The movement of sand and dust particles to the exhaust section is considered as escaped, while the movement of sand and dust particles to the cross-section of the sand discharge outlet is considered as being trapped by the collection box [28]. The sand collection efficiency of the wind erosion instrument is calculated according to Equation (5).

$$Y = \frac{C_1}{C_2} \times 100\% \quad (5)$$

In the formula, C_1 is the number of captured particles collected at the sand outlet, in pieces; C_2 is the total number of particle tracking at the sand inlet, in pieces.

3. Results and Discussion

3.1. Experimental Design and Result Analysis

3.1.1. Single-Factor Experiment

This article mainly discusses the influence of the louver separation device on the sand collection efficiency. Different structural parameters will have different effects on the direction, velocity, and sand collection efficiency of the wind and sand flow entering its interior. The article analyzes the influence of three structural parameters, namely blade inclination angle, blade thickness, and blade number, on the sand collection efficiency of the louver separation device. On the premise of ensuring that the sand collection efficiency of each group is greater than 50% and the airflow velocity at the sand discharge outlet has little disturbance effect on the weighing sensor of the collection box, the horizontal value range of the three factors is initially determined. Then, single-factor simulation experiments are carried out to preliminarily optimize the factor levels and determine the optimal working level range of each factor. The specific factor levels are shown in Table 2.

Table 2. Numerical simulation parameters of wind–sand separator.

Level	Blade Inclination Angle/°	Blade Thickness/mm	Number of Blades/Piece
1	15	0.75	4
2	25	1	7
3	35	1.25	10
4	45	1.5	13
5	55	1.75	16

3.1.2. Single Factor Experiment Results and Analysis

Based on the analysis of experimental data, the impact of various factors on the sand collection efficiency was determined, and the parameter range was further determined. The influence of each single factor on the sand collection efficiency of the wind erosion instrument is shown in Figure 6. As can be seen from Figure 6a, when the blade thickness is set to 1.25 mm and the number of blades is set to 10, with the increase of blade inclination angle, the sand-collecting efficiency shows a trend of first increase and then decrease. When the blade inclination angle is 35°, the sand collection efficiency is the highest. The inclination angle of the blades should not be too large or too small, it should be appropriate. When the inclination angle of the blades is too small and the dust particles are large, it may block the separation device, causing it to accumulate at the louver separation device and reduce the sand collection efficiency; When the inclination angle of the blades is too large, smaller particles of sand and dust can easily enter the lower part through the separation device, resulting in a decrease in blade utilization and the separation device not achieving

the effect of separating sand and dust. Therefore, the range of blade inclination angle should be selected as 25–45°.

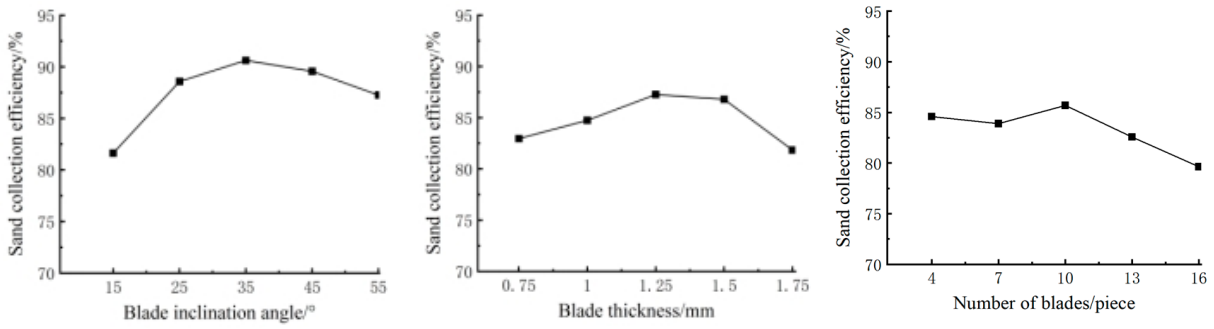

Figure 6. Single-Factor experiment results: (**a**) The influence of blade inclination angle on sand collection efficiency; (**b**) The influence of blade thickness on sand collection efficiency; (**c**) The influence of the number of blades on sand collection efficiency.

Figure 6b shows that when the blade inclination angle is set to 35° and the number of blades is set to 10, with the increase of the blade thickness, its sand collection efficiency shows a trend of firstly increasing and then slowly decreasing. When the blade thickness is 1.25 mm, the sand collection efficiency is the highest. Considering that thin blade thickness during installation and use can affect its load-bearing capacity and cause deformation, thick blades can easily increase weight and resistance, affecting the movement of dust particles and leading to a decrease in efficiency. Therefore, the optimal range for determining blade thickness is 1–1.5 mm.

As can be seen from Figure 6c, when the blade inclination angle is set to 35° and the blade thickness is set to 1.25 mm, with the increase in the number of blades, the sand collection efficiency shows a tendency to increase first and then slowly decrease. The sand collection efficiency is highest when the number of blades is 10. This is because at this time, the sand and dust can generate sufficient airflow between the blades to achieve effective sand and dust capture. If the number of blades is too small, sufficient airflow cannot be generated, which affects the sand collection effect. If there are too many blades, it will lead to an increase in the contact area between dust and blades, resulting in greater resistance and a decrease in sand collection efficiency. Therefore, the optimal range for determining the number of blades should be between 7 and 13.

3.2. Box Behnken Simulation Experiment

Based on the selected range of factors in the single factor simulation experiment, a quadratic regression orthogonal experiment was designed, and the sand collection efficiency was taken as the response value to establish a regression model for the sand collection efficiency of the wind–sand separator, in order to obtain the optimal parameter combination of factors affecting sand collection efficiency [29]. Select the three single factors that have the greatest impact on sand collection efficiency for response surface design [30,31], and the results are shown in Table 3. The Box Behnken experimental design and results are shown in Table 4.

Table 3. Response surface test factor level table.

Level	Blade Inclination Angle/°	Blade Thickness/mm	Number of Blades/Piece
−1	25	1	7
0	35	1.25	10
1	45	1.5	13

Table 4. Box Behnken experimental design and results.

Test Number	A Blade Inclination Angle/°	B Blade Thickness/mm	C Number of Blades/Piece	Y Sand Collection Efficiency/%
1	−1	−1	0	89.74
2	1	−1	0	87.57
3	−1	1	0	93.35
4	1	1	0	86.29
5	−1	0	−1	89.62
6	1	0	−1	85.63
7	−1	0	1	92.51
8	1	0	1	87.26
9	0	−1	−1	84.88
10	0	1	−1	86.69
11	0	−1	1	86.84
12	0	1	1	88.37
13	0	0	0	92.68
14	0	0	0	91.88
15	0	0	0	92.56
16	0	0	0	91.82
17	0	0	0	92.13

3.2.1. Model Establishment and Significance Analysis

Using Design Expert 13 software to conduct variance analysis on the results of sand collection efficiency experiments, the quadratic polynomial regression equation between the simulated sand collection efficiency Y and various experimental factors was obtained as follows: sand collection efficiency (Y) = 92.21 − 2.31A + 0.7088B + 1.02C − 1.22AB − 0.315AC − 0.07BC − 0.4582A^2 − 2.52B^2 − 3C^2.

According to the analysis of variance in Table 5, the model P is less than 0.0001, indicating that the model is extremely significant. The model mismatch term was not significant (p = 0.7080 > 0.05), indicating a high degree of fit in the regression model. If the coefficient of determination R^2 = 0.9937, it indicates a high correlation between the actual value and the predicted value. According to the p-value, the effects of blade inclination angle A, blade thickness B, number of blades C, interaction term AB, and the quadratic terms B^2 and C^2 of blade thickness and number on the sand collection efficiency of the wind erosion instrument are all extremely significant ($p < 0.01$). The quadratic term A^2 of blade inclination angle is significant ($p < 0.05$), while the rest are not significant ($p > 0.05$). The importance of each factor's impact on sand collection efficiency can be determined by the size of the F-value. According to the F-value, the order of the three factors affecting sand collection efficiency is A > C > B; that is, blade inclination angle > number of blades > blade thickness.

Overall, the regression model is extremely significant and can reliably reflect the actual situation, which can be used for further predictive analysis.

3.2.2. Response Surface Analysis

The contour lines and response surface plots of the interaction effects between various factors on sand collection efficiency were created using Design Expert software, as shown in Figure 7. The projection of the response surface graph in the horizontal direction is contour lines. If the contour lines are elliptical, it indicates a significant interaction between these two factors; a circular shape indicates insignificance [32]. In addition, the steepness of the slope of each factor response surface reflects the degree of influence of that factor on sand collection efficiency. The steeper the slope, the greater the impact [33].

Table 5. Variance analysis of regression model for sand collection efficiency.

Variance Source	Sum of Squares	Degree of Freedom	Mean Square	F-Value	*p*-Value	Significance
Model	132.01	9	14.67	122.96	<0.0001	significant **
A	42.64	1	42.64	357.46	<0.0001	**
B	4.02	1	4.02	33.69	0.0007	**
C	8.32	1	8.32	69.77	<0.0001	**
AB	5.98	1	5.98	50.11	0.0002	**
AC	0.3969	1	0.3969	3.33	0.1109	
BC	0.0196	1	0.0196	0.1643	0.6973	
A^2	0.8842	1	0.8842	7.41	0.0297	*
B^2	26.70	1	26.70	223.83	<0.0001	**
C^2	37.91	1	37.91	317.82	<0.0001	**
Residual	0.8350	7	0.1193			
Lack of Fit	0.2243	3	0.0748	0.4897	0.7080	not significant
Pure Error	0.6107	4	0.1527			
Cor Total	132.84	16				
R^2	0.9937					

Note: The F-value is the ratio of two means squared, i.e., the ratio of the effect term to the error term. The larger the F-value, the more significant the difference between the different groups. *p*-value is a probability value used to measure the degree of agreement between the observed data and the original hypothesis. ** indicates that the impact is extremely significant ($p < 0.01$), and * indicates that the impact is significant ($p < 0.05$).

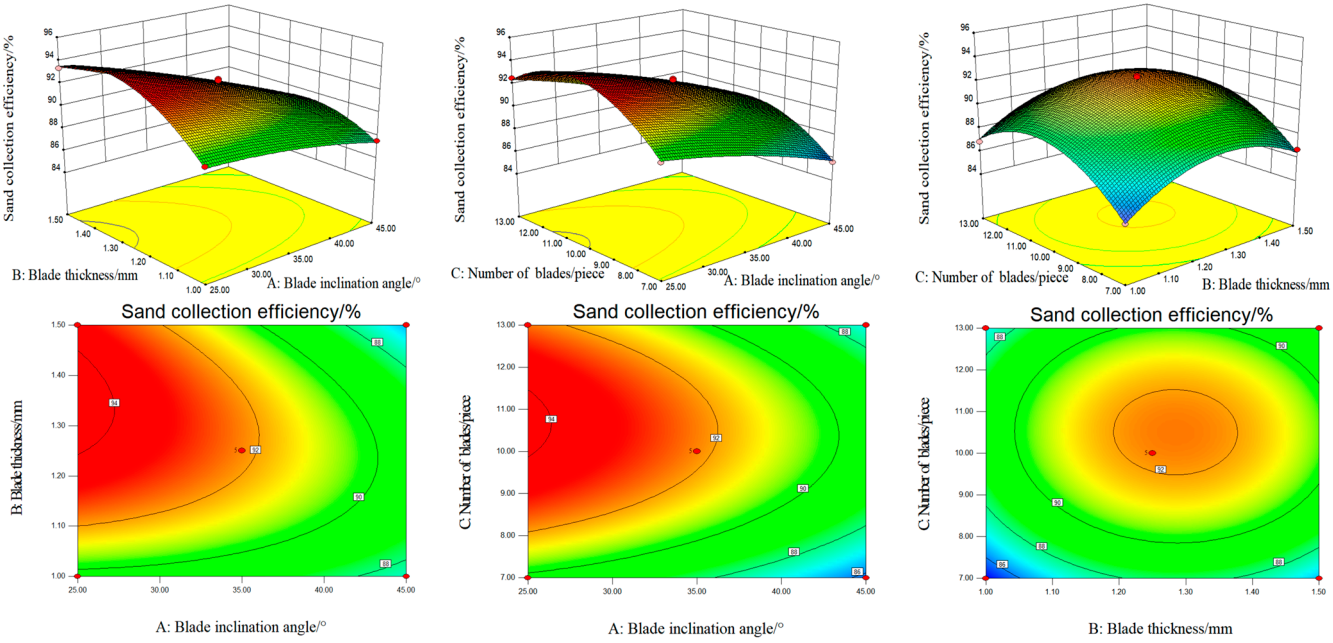

Figure 7. Response surface plot of the interaction effects of various factors on sand collection efficiency.

Figure 7 shows that when the blade inclination angle is certain, the sand collection efficiency shows a trend of increasing and then decreasing with the increase of the blade thickness and the number of blades; when the blade thickness and the number of blades are certain, the sand collection efficiency decreases with the increase of the blade inclination angle. Therefore, in order to improve the sand collection efficiency, the blade inclination angle should not be too large, and the blade thickness and the number of blades should take a moderate value.

3.2.3. Parameter Optimization Experiment

In the optimization module of Design Expert software, the experimental data is optimized and predicted, and the optimal parameter combination is solved with the

maximum sand collection efficiency as the optimization objective value, which is a blade inclination angle of 27.579°, blade thickness of 1.256 mm, and number of blades of 11.063. The optimal solution should be set with a blade inclination angle of 30°, a blade thickness of 1.25 mm, and 10 blades.

4. Analysis of the Influence of Louver Separation Device on the Performance of Wind Erosion Instrument

Based on the differences in flow field and performance, a comparison and analysis were conducted on the internal flow field distribution cloud maps of the wind–sand separator before and after the installation of louver separation devices at x = 0 and y = 0 sections, as well as the relevant data of z = 15 mm (Between the Inlet pipe), z = 70 mm (End of the exhaust pipe), z = 80 mm (Upper end of the Cone shaped deflector), and z = 110 mm (End of the Cone shaped deflector) sections in the z-axis direction (The four cross-sections intercepted are the ones that have a more significant effect on the flow field inside the wind–sand separator before and after the addition of the louver separator).

4.1. Pressure Drop Distribution

The main indicators for evaluating the performance of wind and sand separators are the sand collection efficiency of the separator and the pressure drop of gas passing through the separator. The numerical difference in static pressure inside the separator is the magnitude of the pressure drop, and its variation is often linked to changes in velocity. As shown in Figure 8, the static pressure distribution inside the wind–sand separator varies less along the axial direction and more along the radial direction. In the axial direction, after adding a louver separation device, there is a pressure strip in the shape of a "pendulum tail" from the sand discharge port of the separator to the exhaust port area. In the radial direction, the high-pressure zone occurs at the point where the separator wall and the outer wall of the exhaust pipe generate flow and vortices, while the low-pressure zone occurs inside the exhaust pipe, away from the wall. A strong vortex flow forms a negative pressure zone. In order to improve efficiency, it is necessary to set negative static pressure at the central axis, which helps prevent a large number of small particles from escaping from the outlet into the environment [34]. After the addition of the louver separation device, the negative pressure zone occurs at the center of the cyclone in the wind–sand separator, along the central axis of the wind–sand separator, near the center position inside the exhaust pipe. After adding a louver separation device, the pressure at the exhaust port and sand discharge port of the separator has significantly increased, and the negative pressure phenomenon has been greatly improved, resulting in better sand collection effect.

4.2. Tangential Velocity

Tangential velocity is an important parameter that represents the performance of a wind erosion instrument. The tangential velocity in a wind–sand separator generates centrifugal force, which throws sand particles towards the separator wall, thereby separating the particles from the gas. The higher the tangential velocity, the higher the sand collection efficiency.

From Figure 9, it can be seen that the high-speed zone of the airflow inside the wind–sand separator exists in the area where the outer wall of the exhaust pipe generates cylindrical flow motion. When the airflow passes through the conical guide plate, due to its shape characteristics, the radius of rotation of the airflow decreases, and the tangential velocity of the airflow tends to increase again. There is a low-speed zone near the central axis of the wind–sand separator with an added louver separation device, which coincides with the low-pressure zone in the static pressure distribution. This reflects that the changes in static pressure and flow velocity inside the wind–sand separator are mutually influenced. The results showed that the tangential velocity of the sand separator with added louver separation device was higher than that without louver separation device, which

increased the particle rotation speed and separation performance, and improved the sand collection efficiency.

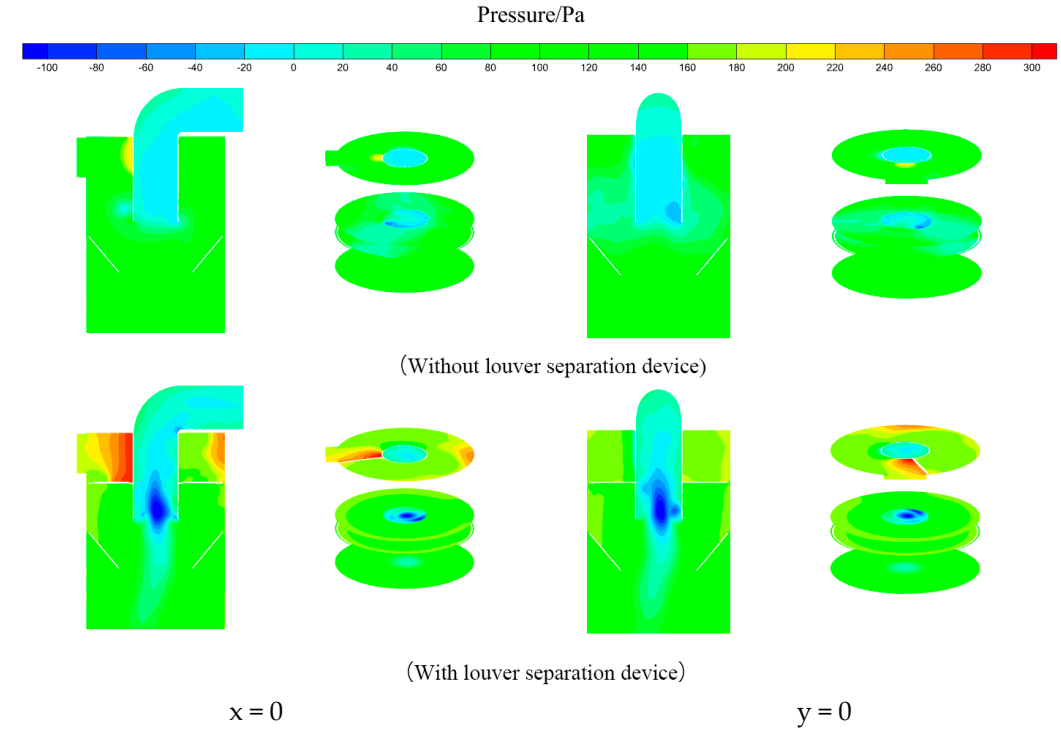

Figure 8. Static pressure distribution inside the wind–sand separator with or without louver separation device.

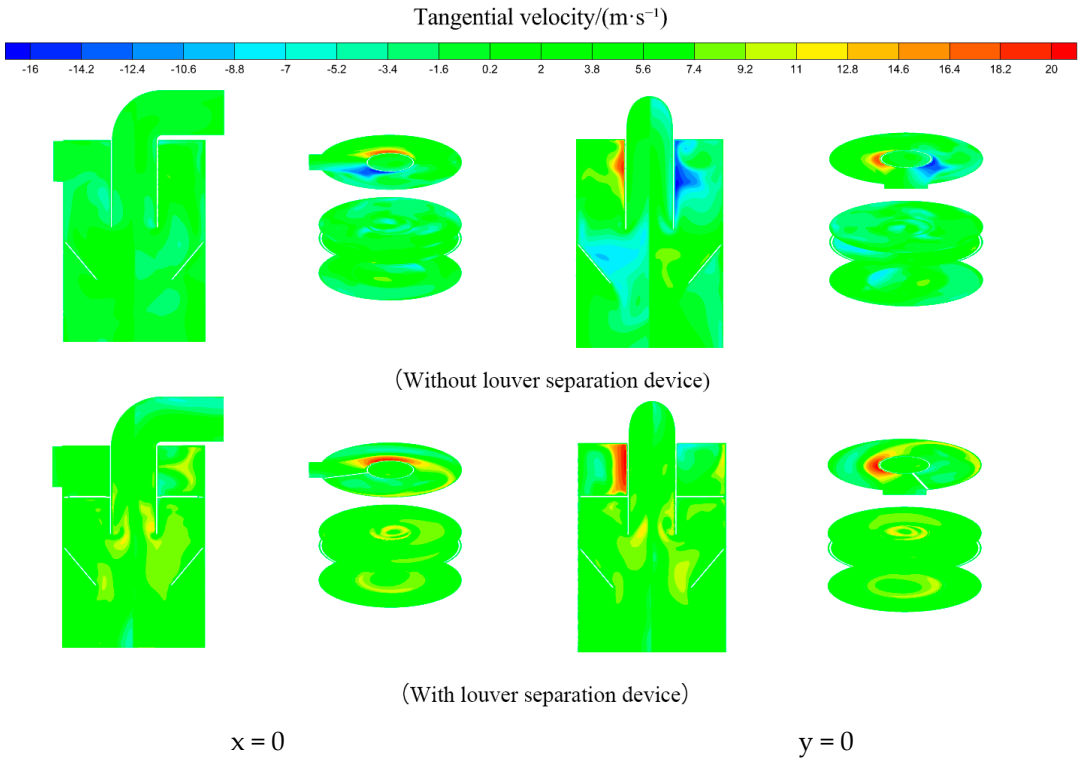

Figure 9. Tangential velocity distribution inside the wind–sand separator with or without louver separation device.

From Figure 10, it can be seen that the tangential velocities of the four sections all exhibit a non-axisymmetric distribution, with the horizontal axis being the ratio of the radial distance r to the circular radius R of the section. At the cross-section of z = 15 mm, the maximum tangential velocity occurs at −0.025R on the curve of the additional louver separation device. This is due to the continuous influx of airflow into the separator at the sand inlet, with a maximum tangential velocity of approximately 20 m/s. In the separation space area between the center and the wall at −0.03R, the addition of a louver separation device in the wind–sand separator has a lower tangential velocity, which promotes particle settling and helps improve sand collection efficiency. As the airflow moves downwards along the wall of the wind–sand separator, the tangential velocity of the airflow decreases and becomes 0 m/s at the edge wall. This is because the frictional force and nonslip boundary conditions between the fluid and the wall help solid particles adhere to the wall until they reach the sand outlet and separate.

X = 0 section tangential velocity

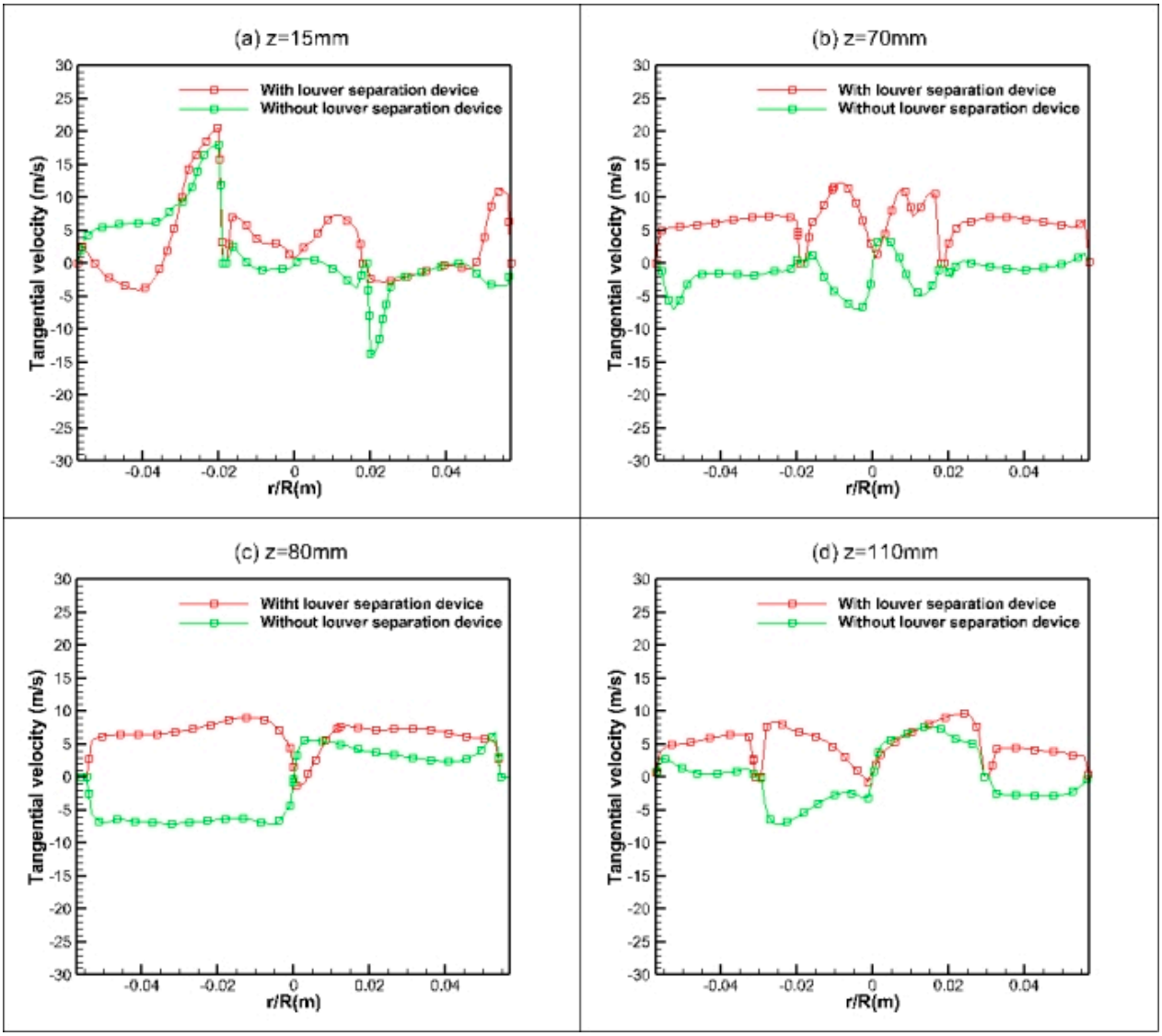

Figure 10. Tangential velocity distribution curves of cross-sections with different z-values.

The tangential velocity of cross-sections z = 70 mm, 80 mm, and 110 mm varies slightly along the axial direction. The separator with an added louver separation device has a higher overall tangential velocity at cross-sections z = 70 mm and z = 110 mm than the

separator without a louver separation device, resulting in higher sand collection efficiency. At the cross-section of z = 80 mm, the separator with the added louver separation device has a lower tangential velocity from the center to the radius of 0.01R, and the trough value of the curve is located at the central axis of the cross-section. The decrease in tangential velocity can suppress the unstable movement of the fluid near the wall and reduce the possibility of solid particles separated by the wall moving upward again. On the contrary, in the remaining separation space areas, the tangential velocity of the separator with added louver separation devices is always slightly higher than that without louver separation devices, which helps to improve sand collection efficiency.

In summary, with the addition of the louver separation device, the tangential velocity shows an overall increasing trend, the centrifugal force of particles increases, the sand collection efficiency improves, and the performance of the wind erosion instrument is improved.

4.3. Axial Velocity

The axial velocity inside the wind–sand separator determines the residence time of sand particles in the separator. After being separated by centrifugal force, the sand particles are discharged from the sand discharge outlet downwards by the axial velocity. There are two vortices inside the wind–sand separator, resulting in two directions of axial velocity. The axial velocity of the outer vortex is downward, which belongs to the downward flow and promotes the downward movement of sand and dust with the outer vortex, which helps to separate the sand and dust. Internal swirling flow belongs to upward flow, moving along the axial direction. The upward axial velocity at the bottom of the separator will cause the separated sand and dust to detach from the collection box with the internal swirling flow, thereby reducing the sand collection efficiency [35]. The exhaust outlet belongs to the upstream flow zone and has a high axial velocity near the outlet, indicating the presence of short-circuit flow at the exhaust outlet. Some of the airflow entering the separator will directly overflow from the exhaust pipe [36], affecting the sand collection efficiency. Therefore, the upward axial velocity should be minimized as much as possible.

From Figure 11, it can be seen that the maximum upward axial velocity at the bottom of the original sand and dust separator is 3.49 m/s, while the maximum upward axial velocity at the bottom of the sand and dust separator with the added louver separation device is 2.22 m/s. The sand and dust separator with the added louver separation device has a smaller overall upward axial velocity, longer particle stagnation time, higher sand collection efficiency, and better performance.

From Figure 12, it can be seen that the axial velocity changes of the four sections are different, and their horizontal axis is the ratio of the radial distance r to the circular radius R of the section. In Figure 12a, the axial velocity at z = 15 mm exhibits a non-axisymmetric distribution with a wavy curve and multiple peak values. According to Figure 12b,c, it can be seen that the maximum valley value of the curve is near the central axis at z = 70 mm and z = 80 mm. With the addition of louver separation devices, the relative increase in axial velocity near the central axis is greater. In Figure 12d, the axial velocity distribution of the original wind–sand separator airflow at z = 110 mm is significantly different from other sections, with upward flow appearing near the central axis, indicating severe backflow at this location. After adding a louver separation device, the upward flow on the central axis disappears, the backflow phenomenon weakens, and the sand collection efficiency improves. Overall, the addition of the louver separation device has improved the reflux phenomenon inside the separator, reduced the short-circuit flow phenomenon, and thus improved the sand collection efficiency.

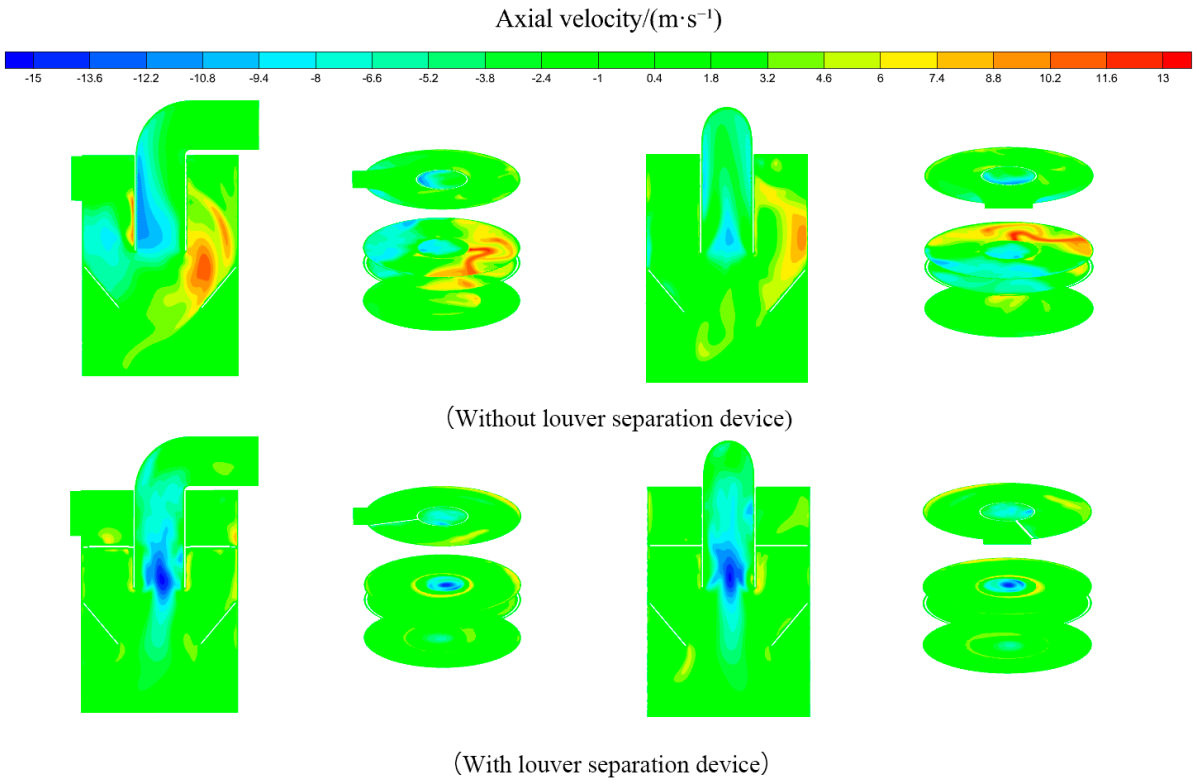

Figure 11. Axial velocity distribution inside the wind–sand separator with or without louver separation device.

4.4. Particle Trajectory

The forces acting on the sand particles in the wind–sand separator mainly include their own gravity, drag force, collision force, etc. Due to the interaction between gas-solid phases in the separator, these forces have a high degree of randomness and complex motion trajectories in the separator. Figure 13 shows the particle movement trajectory of the wind–sand separator before and after the addition of the louver separation device. From the trajectories of the two, it can be seen that the sand particles in the wind–sand flow will be dispersed on the cylindrical wall and nearby areas after entering the separator. Due to the energy loss caused by the collision between the sand particles and the inner wall of the separator and between the sand particles during the rotation of the airflow, the speed of the sand particles decreases, and they move downward along the inner wall of the separator, ultimately completing the separation at the sand discharge outlet.

As shown in Figure 13a, the wind–sand separator without a louver separation device mainly concentrates the movement trajectory of sand particles in the upper half. When the sand particles pass through the lower section of the cylinder, some of the particle movement trajectories will change to upward rotation, resulting in a backflow phenomenon and causing particles to escape from the exhaust pipe, leading to a decrease in sand collection efficiency. As shown in Figure 13b, after adding the louver separation device, the particle trajectory becomes smooth and regular, the intersection point with the wall decreases, the motion trajectory becomes longer, the particles discharged from the exhaust port decrease, and the captured particles increase. This is because the additional frictional force borne by the particles is mainly generated by the blades on the newly added structure, which reduces the particle discharge caused by inner wall friction and helps to prevent dust from being discharged from the exhaust pipe. Meanwhile, after adopting the louver separation device, a continuous spiral path is formed inside the separator, providing sufficient space for particle aggregation and downward movement. The results showed that the sand collection

efficiency and performance of the wind–sand separator were significantly improved and optimized after the addition of the louver separation device.

X = 0 section axial velocity

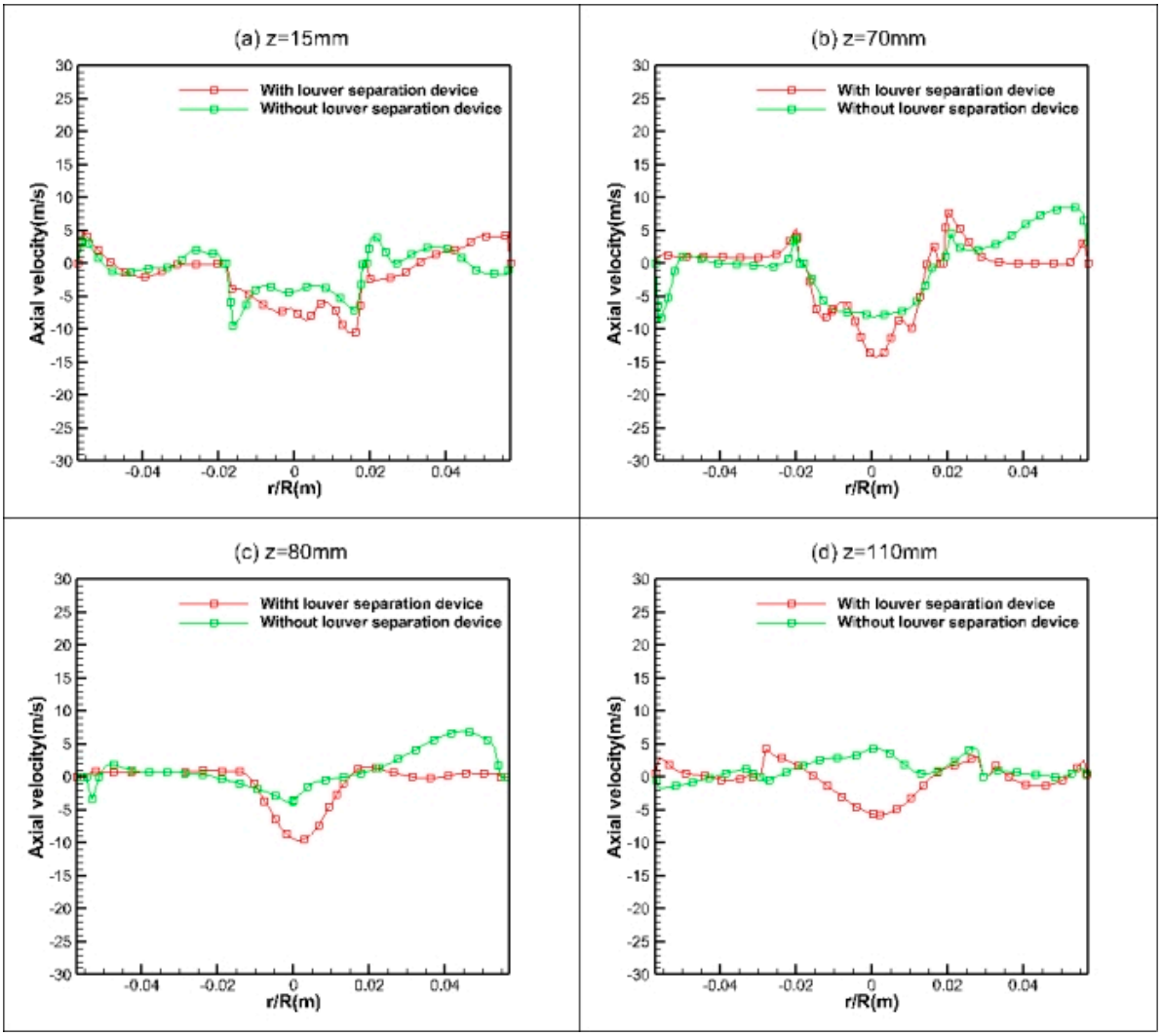

Figure 12. Axial velocity distribution curves of cross-sections with different z-values.

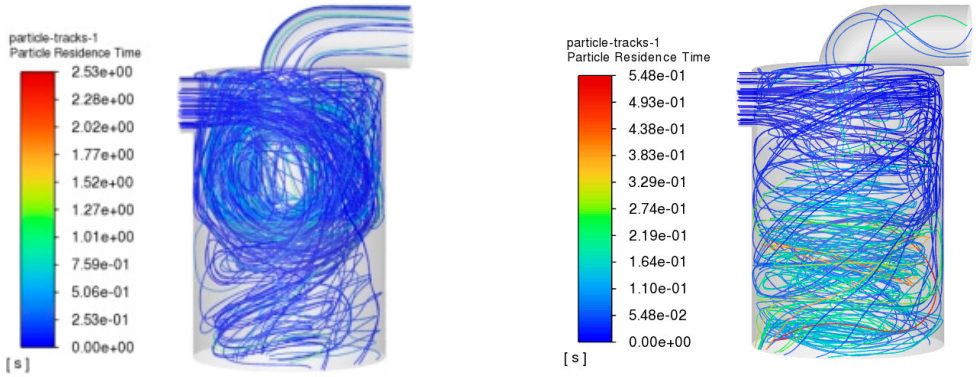

(**a**) (**b**)

Figure 13. Particle trajectory: (**a**) Particle trajectory of wind–sand separator without louver separation device; (**b**) Particle trajectory of wind–sand separator with louver separation device.

4.5. Comparison of Sand Collection Efficiency Within Different Particle Size Ranges

Soil particles are transported in three forms under the action of wind: suspension, jump, and creep [37]. British scholar Bagnold found that dust particles with a particle size less than 0.10 mm are prone to suspension, dust particles with a particle size of 0.10–0.15 mm are prone to jumping, and dust particles with a particle size of 0.15 mm or more are prone to creeping [38]. Research [39] suggests that dust particles with a particle size below 0.075 mm are highly susceptible to being blown away into the atmosphere [40]. Suspended dust particles generally have a particle size less than 0.05 mm, while leaping dust particles typically have a particle size of 0.1–0.5 mm and are the main transport particles for wind erosion. Dust particles with a particle size above 0.5 mm experience gravity greater than air drag and generally do not fly off the surface. Research [41] suggests that fine particles are the key factor affecting soil wind erosion. Based on the above situation, simulations were conducted on particles with diameters between 0.001 and 0.5 mm at a wind speed of 13.8 m/s to obtain trends in sand collection efficiency.

Figure 14 shows the effect of the louver separation device on the sand collection efficiency of the wind–sand separator. The simulation results show that the sand collection efficiency of the separator with the added louver separation device is significantly higher than that without the louver separation device. In addition, for particles with diameters of 0.001–0.005 mm, 0.005–0.01 mm, 0.01–0.05 mm, 0.05–0.1 mm, and 0.1–0.5 mm, the sand collection efficiency of the wind–sand separator increased from 52.45%, 59.91%, 67.8%, 87.63%, and 99.79% to 69.62%, 73.42%, 90.29%, 97.66%, and 99.92%, respectively, after adding a louver separation device. The average sand collection efficiency was 86.18%.

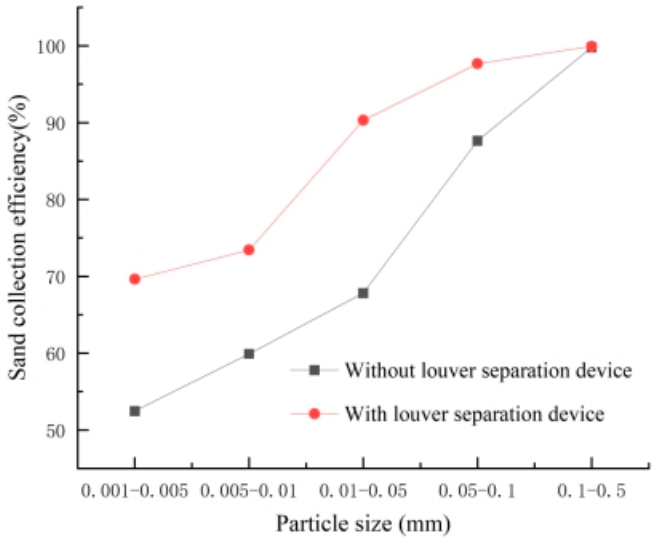

Figure 14. Sand collection efficiency curve of wind–sand separator with or without louver separation device.

5. Wind Tunnel Experiment Verification

5.1. Preparation for the Experiment

Conduct performance tests on the wind–sand separator using a self-made micro wind tunnel in the Transportation Laboratory of Jilin Agricultural University to verify the accuracy of its simulation results. The wind tunnel test is conducted at atmospheric pressure without external wind interference. Using acrylic round tubes and 3D printing technology to produce a physical device for wind–sand separators. The inlet velocity of the inlet pipe is jointly controlled by the fan and frequency converter in the micro wind tunnel. The wind and sand flow situation and physical device are shown in Figure 15.

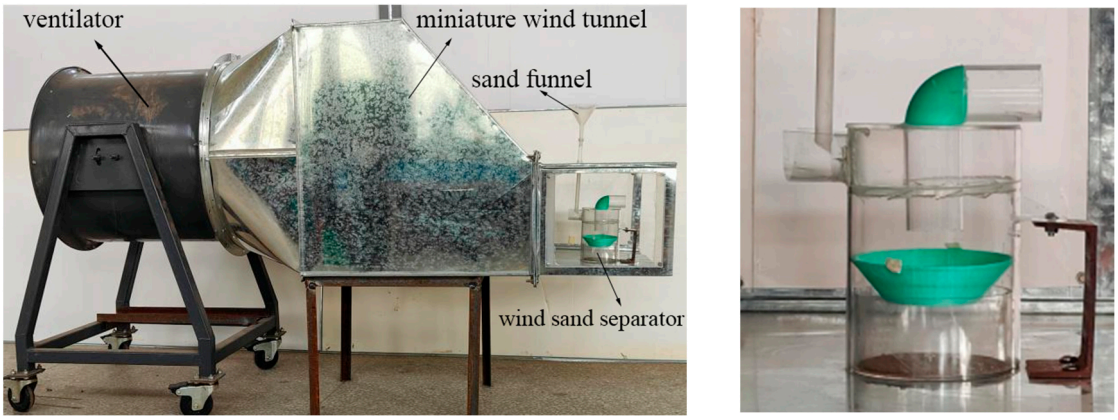

(**a**) (**b**)

Figure 15. Wind–sand separation performance test diagram: (**a**) Experimental diagram of micro wind tunnel; (**b**) Physical picture of wind–sand separator.

5.2. Sand Collection Efficiency Test

The experimental soil sample was taken from Wohu Town, Shuangliao City. Prior to the experiment, the soil sample was naturally dried, and the moisture content of the naturally dried soil sample was measured to be 1.47% using a constant temperature oven drying method. Sift out a mixed soil sample with a particle size of less than 0.5 mm from the soil sample for testing purposes. Design a sand inlet at the front end of the air inlet pipe of the sand separator, and fix the sand funnel at the sand inlet. Turn on the fan and wait for the wind speed in the test section to reach the predetermined wind speed of 13.8 m/s before starting to transport soil samples. Take 50 g of soil sample for each test and record the sand collection situation of the wind erosion instrument. After the soil sample is transported, turn off the fan, weigh and record the soil sample in the collection box, repeat the experiment three times under the optimal parameter combination according to the above steps, take the average value, and observe the sand collection efficiency of the wind erosion instrument.

5.3. Testing Results and Analysis

Using the gas–solid separation efficiency η as the sand collection efficiency, that is, the ratio of the mass M_0 of the farmland soil sample collected in the collection box to the mass M of the farmland soil sample entering the wind–sand separator during the experiment, calculate the sand collection efficiency according to Equation (6).

$$\eta = \frac{M_0}{M} \times 100\% \tag{6}$$

Under the optimal parameter combination, according to Equation (6), when the inlet velocity of the inlet pipe is 13.8 m/s, the sand collection efficiency of the wind erosion instrument's sand separator is 68.49%, 71.23%, 88.15%, 95.47%, and 98.26%, respectively, with an average value of 84.32% and an average error of 2.2% compared to the simulation value. The sand collection efficiency results of the optimized wind erosion instrument simulation test and wind tunnel test are shown in Figure 16, which can intuitively compare the sand collection efficiency of the two. The error between the two is small, which verifies the reliability of the numerical simulation and verifies the effect of the optimized design of the wind erosion instrument structure.

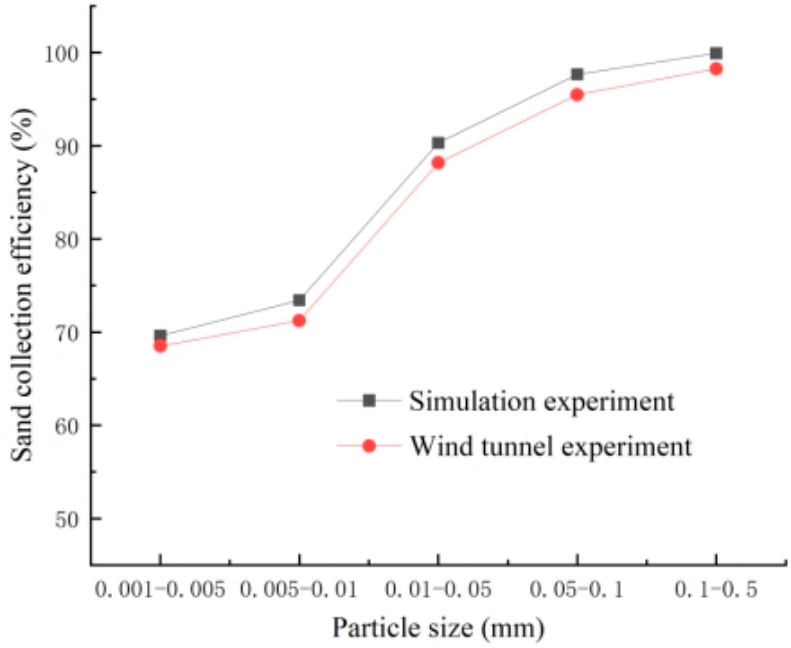

Figure 16. Comparison of sand collection efficiency between wind erosion instrument simulation test and wind tunnel test.

The reason for the error between the experimental values of sand collection efficiency and the numerical simulation values is that the accuracy of the processed products is insufficient, such as the roughness of the surface and joints of 3D printed parts, and the significant error in the bonding size, which affects the simulation results.

6. Limitations and Future Research Directions

In this study, the sand collection efficiency of the wind erosion instrument is improved by adding a louvered separation device inside the wind–sand separator. The structure of the wind erosion instrument is simulated and analyzed by CFD and Fluent 2022 software, the numerical simulation is carried out by using the RNG k-ε model, and the discrete phase modeling (DPM) method is applied to calculate the sand collection efficiency of the wind erosion instrument. The changes in the sand collection efficiency and performance of the wind erosion instrument before and after the addition of the louver separation device were compared, and finally, the optimized structure was assembled and micro wind tunnel tests were conducted to verify the reliability of the simulation model. The results show that the addition of a louver separation device in the wind–sand separator can significantly improve the sand collection efficiency of the wind erosion instrument, which can provide a theoretical basis for related research.

It should be noted that there are some limitations in this study, which mainly takes the soil wind erosion in the Shuangliao area of Jilin Province as an example, investigates the common wind speed and particle size of wind erosion in this area, and optimizes the structure of wind erosion instrument on this basis. However, there are some differences in wind erosion in different regions, so the results of this study may not be applicable to other regions. In the future, we will analyze the wind erosion conditions in different regions and combine the automatic weighing system with the wind–sand separator to achieve automatic weighing of the overall structure of the wind erosion instrument in order to further improve the accuracy and reliability of the monitoring of wind erosion and thus ensure the versatility and flexibility of the wind erosion instrument when used in different regions.

7. Conclusions

This article improves the performance and sand collection efficiency of the wind erosion instrument by installing a louver separation device inside the wind–sand separator. The main conclusions are as follows:

(1) Using CFD and Fluent software, single-factor simulation analysis and response surface testing were conducted using numerical simulation methods. Based on the premise of maximizing sand collection efficiency, the optimal blade inclination angles are 25°, 35°, and 45°, blade thicknesses are 1, 1.25, and 1.5 mm, and the number of blades is 7, 10, and 13. The structural parameter range of the louver separation device is determined. Based on the response surface test results, the optimal parameter combination was obtained as follows: blade inclination angle of 30°, blade thickness of 1.25 mm, and ten blades. The factors affecting sand collection efficiency are in the order of blade inclination angle > number of blades > blade thickness.

(2) The performance of the wind–sand separator before and after the addition of the louver separation device was compared. The results showed that compared with the sand separator without the louver separation device, the sand separator with the added louver separation device had higher internal static pressure, lower flow loss, and a more stable flow field; As the tangential velocity increases, the centrifugal force of particles also increases, and the amount of particle escape decreases, which is beneficial for capturing particles; The overall axial velocity in the separation center area is reduced, which prolongs the residence time of gas inside, improves the reflux phenomenon, and makes the particle trajectory smoother and more regular, mostly in a spiral motion. The intersection point with the wall is reduced, which helps to improve the sand collection efficiency.

(3) Compared with the wind–sand separator without a louver separation device, the wind–sand separator with a louver separation device has higher sand collection efficiency. For particles with diameters of 0.001–0.005 mm, 0.005–0.01 mm, 0.01–0.05 mm, 0.05–0.1 mm, and 0.1–0.5 mm, the sand collection efficiency of the wind–sand separator increased from 52.45%, 59.91%, 67.8%, 87.63%, and 99.79% to 69.62%, 73.42%, 90.29%, 97.66%, and 99.92%, respectively, after adding a louver separation device. The sand collection efficiency increased by 32.74%, 22.55%, 33.17%, 11.45%, and 0.13%, respectively. When the wind speed is 13.8 m/s and the diameter range is 0.001–0.5 mm, the average sand collection efficiency obtained from simulation tests and wind tunnel tests is 86.18% and 84.32%, respectively, with an error of 2.2%, which is relatively small. This verifies the reliability of the simulation results and verifies the effect of structural optimization design, providing a basis for improving the performance of the wind erosion instrument.

In summary, the wind erosion meter can effectively separate and capture sand and dust particles in the process of wind erosion so as to accurately measure the intensity and frequency of the occurrence of wind erosion, reduce the occurrence of the phenomenon of wind erosion, and provide more effective ecological and environmental monitoring measures for the areas where wind erosion phenomena are frequent, and thus maintain the sustainable development of the environment.

Author Contributions: Conceptualization, Z.L., X.M. and M.A.; methodology, Z.L., X.M., F.Z. and D.H.; software, Y.M. and D.H.; validation, Z.L. and X.M.; formal analysis, Z.L., X.M., F.Z. and D.H.; investigation, X.M.; resources, X.M.; data curation, Z.L. and X.M.; writing—original draft preparation, Z.L.; writing—review and editing, X.M. and D.H.; visualization, Z.L. and X.M.; supervision, X.M.; project administration, X.M., D.H. and M.A.; funding acquisition, X.M. All authors have read and agreed to the published version of the manuscript.

Funding: This research was funded by the National Key Research and Development Program of China (2023YFD1500404) and the Changchun Science and Technology Development Plan Project (21ZGM04).

Institutional Review Board Statement: Not applicable.

Informed Consent Statement: Not applicable.

Data Availability Statement: The data presented in this study are available from the corresponding author upon reasonable request.

Acknowledgments: In this paper, we received technical support from the College of Biological and Agricultural Engineering at Jilin University, including the Licensed software of Fluent.

Conflicts of Interest: The authors declare no conflicts of interest.

Nomenclature

a	Inlet pipe diameter (mm)
B	Inlet pipe length (mm)
L	Insertion depth of exhaust pipe (mm)
S	Cone shaped deflector height (mm)
D	Cylinder length (mm)
d	the hydraulic diameter (m)
A	Blade inclination angle (°)
B	Blade thickness (mm)
C	Number of blades (piece)
M_0	The quality of farmland soil samples collected by the collection box after the test (g)
M	Mass of farmland soil samples entering the wind–sand separator during the tes (g)
X	section position in x direction (mm)
Y	section position in y direction (mm)
Z	section position in z direction (mm)
r	radial position (m)
R	Section circle radius (m)
η	Sand collection efficiency (%)

References

1. Chen, Z.; Ma, S. Research on hazards and control strategies of farming soil wind erosion in the arid and semi-arid region. *J. Inn. Mong. Univ. Natl. Nat. Sci.* **2006**, *2*, 159–164.
2. Chen, S.; Dong, Y. A review of the research on wind erosion climatic erosivity. *J. Desert Res.* **2020**, *40*, 65.
3. Webb, N.P.; Herrick, J.E.; Van Zee, J.W.; Courtright, E.M.; Hugenholtz, C.H.; Zobeck, T.M.; Okin, G.S.; Barchyn, T.E.; Billings, B.J.; Boyd, R.; et al. The National Wind Erosion Research Network: Building a standardized long-term data resource for aeolian research, modeling and land management. *Aeolian Res.* **2016**, *22*, 23–36. [CrossRef]
4. Hairu, W. Analysis and research on the causes of sandstorm in China. *Environ. Dev.* **2020**, *32*, 170–171.
5. Chen, Z.; Ma, S.; Zhao, Y.; Sun, Y.; Cui, H. Characteristics of drifting sand flux over conservation tillage fiel. *Trans. Chin. Soc. Agric. Eng.* **2010**, *26*, 118–122.
6. Giambastiani, Y.; Giusti, R.; Gardin, L.; Cecchi, S.; Iannuccilli, M.; Romanelli, S.; Bottai, L.; Ortolani, A.; Gozzini, B. Assessing Soil Erosion by Monitoring Hilly Lakes Silting. *Sustainability* **2022**, *14*, 5649. [CrossRef]
7. Sun, Y.; Ma, S.; Chen, Z.; Zhao, Y.; Dong, M. In situ testing on soil erosion of grassland surface in the northern farming-pastoral zone. *Trans. Chin. Soc. Agric. Mach.* **2010**, *41*, 49–52.
8. Feng, X.; Gao, H.; Li, H.; Wang, X.; Ma, H. Effect of wind erosion in agro-pastoral regions on soil characteristics. *Trans. Chin. Soc. Agric. Mach.* **2007**, *38*, 51–54.
9. Wang, J.; Zhao, M. Sand sampler research analysis and reflection. *J. Agric. Mech. Res.* **2008**, *5*, 216–218.
10. Shang, X.; Chen, Z.; Song, T.; Chang, J.; Qiu, Y.; Chen, L. Numerical Simulation and Deceleration Performance Analysis of Soil Wind Erosion Sand Sampler. *Soil Water Conserv. China* **2017**, 38–41. [CrossRef]
11. Cui, Y.; Guo, Z.; Chang, C.; Wang, R.; Li, J. A Continuous-weighing Sand Trap: Design and field evaluations. *J. Desert Res.* **2018**, *38*, 1166.
12. Dong, Z.; Zheng, X. Research Achievements in Aeolian Physics in China for Last Five Decades (II). *J. Desert Res.* **2005**, *25*, 795–815.
13. Bagnold, R.A. *The Physics of Blown Sand and Desert Dunes*; Methuen and Company Limited: North Yorkshire, UK, 1941.
14. Fryrear, D.W. A field dust sampler. *J. Soil Water Conserv.* **1986**, *41*, 117–120.
15. Kuntze, H.; Beinhauer, R.T.; Tetzlaff, G. Quantifizierung der bodenerosion durch wind. *Mitt. Dt. Bodenkundl. Ges.* **1989**, *59*, 1089–1094.
16. Goossens, D.; Offer, Z.Y. Wind tunnel and field calibration of six aeolian dust samplers. *Atmos. Environ.* **2000**, *34*, 1043–1057. [CrossRef]

17. Song, T.; Chen, Z.; Ma, Q.; Si, Z.; Liu, H.; Xuan, C. Design and performance experiment of shunt-hedging sand sampler. *Trans. Chin. Soc. Agric. Mach.* **2015**, *46*, 173–177.
18. Gao, Z.; Wang, J.; Wang, J.; Ma, Z.; Mao, Y.; Wei, Y. Progress in the application of internal components in cyclone separator. *Acta Petrol. Sin.* **2019**, *35*, 393–402.
19. Wang, F. *Computational Fluid Dynamics Analysis: The Principle and Application of the CFD Software*; Tsinghua University Press: Beijing, China, 2004; pp. 160–195.
20. Hou, J. Study on Cyclone Separator of High Pressure System. Master Thesis, Tianjin University, Tianjin, China, 1 June 2012.
21. Liu, S.Y.; Zhang, Y.; Wang, B.G. Cyclone separator three-dimensional turbulent flow-field simulation using the Reynolds stress model. *Trans. Beijing Inst. Technol.* **2005**, *5*, 377–379.
22. Li, Q.; Xu, Y.; Du, L.; Xie, J.; Cheng, J.; Wang, Y. Numerical simulation of JLX cyclone separator with guiding vane. *Chin. J. Chem. Eng.* **2015**, *43*, 37–41.
23. Wang, Y.; Liu, Y.; Miao, G. Three-dimensional numerical simulation of viscous flow around circular cylinder. *J. Shanghai Jiaotong Univ. Chin. Ed.* **2001**, *35*, 1464–1469.
24. Li, J. Retrospects and prospects of fluid mechanics. *Adv. Mech.* **1995**, *25*, 442–450.
25. Sun, Z.; Wu, X. Discussion and application of CFD numerical simulation technology. *Water Conserv. Sci. Technol. Econ.* **2008**, *14*, 126–128.
26. Zhang, L.; Li, J.; Chang, C.; Guo, Z.; Liu, j.; Wang, R.; Li, Q.; Wang, X. Influence of spatial-temporal resolution of wind speed data on calculation result of soil wind erosion modulus. *J. Desert Res.* **2022**, *42*, 21.
27. Tao, S. Study on Inner Flow-Field Characteristics and Shunt-Hedging and Multi-Stage Expansion Combined Automatic Sand Sampler. PhD Thesis, Mongolia Agricultural University, Hohhot, China, 1 July 2016.
28. Tan, L.; Yuan, Y.; Huang, C.; Yu, Q.; Tang, L.; Dong, J. Numerical simulation on flow field analysis and structure optimization of a cyclone separator. *J. Shaanxi Univ. Sci. Technol.* **2018**, *36*, 152–159.
29. Hou, J.; Zhang, E.; Sun, Y.; Zhang, L.; Zhou, K. Structural optimization and performance analysis of button pressure-compensating emitters. *Trans. CSAE* **2022**, *38*, 100–108.
30. Qu, M.; Zhao, S.; Zhu, X.; Wan, Z.; Liu, L.; Huang, Y.; Zhu, Y.; Yang, X. Optimization of Microwave-Hot Air Dehydration Process and Quality Evaluation of Frozen Tofu by Response Surface Methodology. *Sci. Technol. Food Ind.* **2021**, *42*, 158–166.
31. Sun, Q.; Cheng, Y.; Yang, G.; Ma, Z.F.; Zhang, H.; Li, F.; Kong, L. Stability and sensory analysis of walnut polypeptide liquid: Response surface optimization. *Int. J. Food Prop.* **2019**, *22*, 853–862. [CrossRef]
32. Li, Y.; Yang, X.; Liu, J.; Wu, J.; Wang, Z.; Zhang, X. Ultrasonic-assisted alkaline extraction of Plukenetia volubilis protein isolate and its processing properties. *Food Ferment. Ind.* **2021**, *47*. (In Chinese) [CrossRef]
33. Ye, X.; Cheng, S.; Wen, L.; Zeng, X.; Zhou, G. Optimization of fermentation technology for mulberry wine by response surface methodology. *China Brew.* **2017**, *36*, 105–109.
34. Sardar, R.; Oh, J.; Kim, M.; Lee, J.-E.; Kim, S.; Kim, K.C. The effect of inlet velocity, gas temperature and particle size on the performance of double cyclone separator. *Chem. Eng. Process. Process Intensif.* **2023**, *191*, 109469. [CrossRef]
35. Huang, Y.; Zhao, M. Optimization design of performance test of cyclone separator sand sampler based on numerical simulation and wind erosion tunnel experiment. *Trans. Chin. Soc. Agric. Eng.* **2015**, *31*, 50–56.
36. Qing, Y. Numerical Simulation and Optimization on Gas-Solid Flow Characteristics of the Sand Trap. Master Thesis, Wuhan University of Technology, Wuhan, China, 1 March 2021. [CrossRef]
37. Meng, Q.; Chen, Z.; Hao, B.; Niu, W.; Cui, H.; Wang, W. Performance Comparison Test of Split–flow Hedging and Cyclic Friction Farm Sand Separator. *J. Agric. Mech. Res.* **2020**, *42*, 169–174.
38. Bagnold, R.A. *The Physics of Blown Sand and Desert Dunes*, Reprint ed.; Courier Corporation: North Chelmsford, MA, USA, 2012.
39. Li, X.; Shen, X.; Xie, W. Analysis of dynamic characteristics of sand grains in wind erosion soil. *Trans. Chin. Soc. Agric. Eng.* **2009**, *25*, 71–75.
40. Ma, S.; Chen, Z. *Soil Wind Erosion Testing and Control Technology*; Science Press: Beijing, China, 2010.
41. Yuan, Z.; Zhu, L.; Geng, F.; Peng, Z.; Zhang, X. *Gas Solid Two Phase Flow and Numerical Simulation*; Nanjing Southeast Univ. Press: Nanjing, China, 2013; Volume 201302, p. 196.